Video Article

Phosphorus-31 Magnetic Resonance Spectroscopy: A Tool for Measuring *In Vivo* Mitochondrial Oxidative Phosphorylation Capacity in Human Skeletal Muscle

Vidhya Kumar[1], Henry Chang[1], David A. Reiter[2], David P. Bradley[3], Martha Belury[4], Shana E. McCormack[5], Subha V. Raman[1]

[1]Davis Heart and Lung Research Institute, The Ohio State University

[2]Laboratory of Clinical Investigation, National Institute on Aging

[3]Division of Endocrinology, Diabetes and Metabolism, The Ohio State University

[4]Department of Human Sciences, Human Nutrition, The Ohio State University

[5]Division of Endocrinology and Diabetes, Department of Pediatrics, University of Pennsylvania

Correspondence to: Subha V. Raman at subha.raman@osumc.edu

Abstract

Skeletal muscle mitochondrial oxidative phosphorylation (OXPHOS) capacity, which is critically important in health and disease, can be measured *in vivo* and noninvasively in humans via phosphorus-31 magnetic resonance spectroscopy (^{31}PMRS). However, the approach has not been widely adopted in translational and clinical research, with variations in methodology and limited guidance from the literature. Increased optimization, standardization, and dissemination of methods for *in vivo* ^{31}PMRS would facilitate the development of targeted therapies to improve OXPHOS capacity and could ultimately favorably impact cardiovascular health. ^{31}PMRS produces a noninvasive, *in vivo* measure of OXPHOS capacity in human skeletal muscle, as opposed to alternative measures obtained from explanted and potentially altered mitochondria via muscle biopsy. It relies upon only modest additional instrumentation beyond what is already in place on magnetic resonance scanners available for clinical and translational research at most institutions. In this work, we outline a method to measure *in vivo* skeletal muscle OXPHOS. The technique is demonstrated using a 1.5 Tesla whole-body MR scanner equipped with the suitable hardware and software for ^{31}PMRS, and we explain a simple and robust protocol for in-magnet resistive exercise to rapidly fatigue the quadriceps muscle. Reproducibility and feasibility are demonstrated in volunteers as well as subjects over a wide range of functional capacities.

Video Link

The video component of this article can be found at https://www.jove.com/video/54977/

Introduction

The goal of this work is to outline a reproducible method to noninvasively measure *in vivo* skeletal muscle mitochondrial function in individuals possessing a wide range of abilities. Aberrant mitochondrial impairment is a hallmark of a wide range of metabolic syndromes and genetic diseases, from common conditions such as aging and diabetes to rare disorders such as Friedreich's ataxia.

Metabolic Syndrome and Mitochondrial Dysfunction

Metabolic syndrome has been shown to disrupt mitochondrial function, depress skeletal muscle OXPHOS, and lead to ectopic lipid storage in skeletal muscle[1,2]. As critical organelles regulating metabolic and energy homeostasis, mitochondria are implicated in the pathophysiology of obesity[3,4], insulin resistance[5], Type 2 Diabetes Mellitus (*T2DM*)[6,7], diabetes-related micro-[8,9,10,11] and macrovascular complications[12,13], and non-alcoholic fatty liver disease (NAFLD)[14,15,16], among others. Insulin resistance is characterized by profound changes in skeletal muscle mitochondrial activity, including decreased mitochondrial tricarboxylic acid (TCA) flux rate, ATP synthesis rate, and citrate synthase and NADH:O_2 oxidoreductase activity[5]. One hypothesis is that these alterations could be due to the accumulation of free fatty acid (FFA) metabolites in the muscle, which are markedly augmented during obesity and other obesity-related diseases[2,17]. The exposure of muscle to elevated FFAs and lipid intermediates can decrease the expression of genes in the lipid oxidative pathway as well as the TCA cycle and electron-transport chain (ETC)[18]. This reduction in mitochondrial skeletal muscle OXPHOS capacity in the setting of a lipid overload is accompanied by a decline in the quantitative (content and biogenesis of mitochondria)[19] and qualitative function of skeletal muscle mitochondria[20]. Exposing skeletal muscle and myocytes to FFAs leads to severe insulin resistance, and increased FFA uptake in muscle is associated with insulin resistance in both humans and rodents[21]. The lipid intermediates ceramide and diacylglycerol (DAG) have been shown to directly inhibit the insulin signaling pathway by altering the activity of kinases, such as protein kinase C and protein kinase B[21]. Therefore, lipid-derived molecules appear to play a prominent

role in the development of skeletal muscle insulin resistance and T2DM. However, it remains unclear whether changes in mitochondrial capacity are a cause or a consequence of insulin resistance[22].

Friedrich's Ataxia and Mitochondrial Dysfunction

Decreased OXPHOS can also arise from genetic defects. Friedrich's ataxia (FA), the most common form of hereditary ataxia, is a genetic disorder caused by a mutation in the frataxin (FXN) gene, resulting in intra-mitochondrial iron accumulation, reactive oxygen species production, and abnormalities of oxidative phosphorylation[23,24,25,26]. This important discovery has led to the development of targeted therapies, which aim to improve mitochondrial function at the sub-cellular level. Despite this understanding, there has been limited development of *in vivo*, reproducible biomarkers for FA clinical research. In fact, a critical barrier in the effective evaluation of targeted therapies in FA is the inability to track changes in mitochondrial function. Current functional measures, for example, can identify decreased cardiac output; however, they are incapable of determining the level at which the dysfunction occurs (**Figure 1**). The development of a reliable marker of mitochondrial function that can be used to identify and evaluate disease progression in Friedrich's ataxia is crucial to gauge the relevant mechanistic impact of targeted therapies.

Impaired OXPHOS and Cardiac Dysfunction

Aberrant mitochondrial function, either acquired or genetic, could contribute to the development or progression of cardiac dysfunction. Under the conditions of pressure overload and heart failure, the primary energy substrate preference switches from FFA to glucose. This is associated with decreased ETC activity and oxidative phosphorylation[27]. The pathophysiology of mitochondrial bioenergetics in cardiac dysfunction can be different depending on the primary origin of the mitochondrial defect. Diabetes and metabolic syndrome results in mitochondrial abnormalities in myocardium, such as impaired biogenesis and fatty acid metabolism, which lead to reduced substrate flexibility, energy efficiency, and eventually, diastolic dysfunction[28,29]. In FA, on the other hand, a frataxin deficiency results in significant mitochondrial iron accumulation in cardiomyocytes[30,31]. Iron accumulation leads to the production of free radicals via the Fenton reaction[32] and increases the chance of free radical-induced cardiomyocyte damage. Intra-mitochondrial iron accumulation is also associated with an increased sensitivity to oxidative stress and a reduced oxidative capacity[30,31]. Iron accumulation and subsequent aberrant mitochondrial function, due to frataxin deficiency, may therefore be responsible for the impaired cardiac energetics and cardiomyopathy observed in FA[33,34]. It is also interesting to note that the reduced oxidative capacity in skeletal muscle mitochondria parallels the exercise intolerance and reduced metabolic capacity in heart failure (HF)[35]. Measurement of skeletal muscle OXPHOS capacity, as detailed herein, is readily implementable and robust; coupled with the significance of skeletal muscle OXPHOS in HF, these features make it an appealing biomarker in comprehensive studies of heart disease[36].

Impaired OXPHOS and the accompanying cardiac dysfunction is not an inconsequential aspect of metabolic and mitochondrial disease. Subjects with diabetes and metabolic disease are at a higher risk of developing cardiovascular disease and have excess mortality after myocardial infarction (MI)[37,38,39,40,41]; over half of FA subjects have cardiomyopathy, and many die of cardiac arrhythmia or heart failure[42]. Therefore, quantification of reduced OXPHOS could not only allow for early detection and treatment of cardiac dysfunction, but it could also alleviate a major clinical burden in these diseases.

Targeted therapies to directly increase OXPHOS capacity is a promising area to improve the treatment of subjects, whether the cause of metabolic dysfunction is genetic or acquired. Currently, the development of novel targeted drugs that either alleviate abnormal mitochondrial function[43] or correct the primary genetic defect[44] can improve the deranged bioenergetics characteristic of FA. In the case of acquired mitochondrial dysfunction, increased physical activity can improve mitochondrial function[45,46,47].

[31]Phosphorous Magnetic Resonance Spectroscopy as a Non-invasive Biomarker of Mitochondrial Function

Regardless of the tested therapy, an integrated *in vivo* assessment of skeletal muscle bioenergetics is a crucial tool to assess the impact of targeted interventions, especially in subjects with severe exercise intolerance or the inability to undergo conventional metabolic testing. Magnetic resonance spectroscopy tuned to phosphorous (^{31}PMRS), an endogenous nucleus found in various high-energy substrates within cells throughout the body, has been used to quantify mitochondrial oxidative capacity using a variety of approaches, including in-magnet exercise-recovery protocols and muscle stimulation protocols[48]. The exercise-recovery protocols rely upon a variety of apparatus ranging in complexity from MRI-compatible ergometers that regulate and measure workload to simple configurations of straps and pads allowing for burst-type resistive and quasi-static exercise. One of the primary goals of any of these protocols is to produce an energy imbalance for which the demand for adenosine triphosphate (ATP) is initially met through the enzymatic breakdown of phosphocreatine (PCr) through the creatine kinase reaction[49]. Upon cessation of exercise, the rate of ATP production is dominated by oxidative phosphorylation and represents the maximum *in vivo* capacity of the mitochondria[50]. Furthermore, OXPHOS during post-exercise recovery can be described by a first-order rate reaction[51]. The post-exercise recovery of PCr can therefore be quantified by the fitting of an exponential time constant (τ_{PCr}), with smaller values of τ_{PCr} representing greater capacities for oxidative ATP synthesis. Significant efforts have been made to validate ^{31}PMRS against *ex vivo* and more direct measures of OXPHOS and demonstrate the potential clinical applicability of this technique[52,53,54,55].

Notably, the protocol described in this work can be implemented on clinically-available scanners, and it has been widely validated as a noninvasive biomarker of mitochondrial function[56]. However, an exercise ^{31}PMRS protocol optimized for application to individuals with varying severities of neuromuscular impairment or mobility has not been well established[57]. A well-defined, broadly-applicable exercise protocol and ^{31}PMRS technique would be particularly useful in the evaluation of diseases with fundamental abnormalities in mitochondrial function.

Several prior studies have explored the applications of non-invasive techniques to quantify mitochondrial function in subjects. For instance, these techniques have shown impaired OXPHOS in subjects with type 2 diabetes[36]. Lodi *et al.* first tested the feasibility of PMRS techniques in subjects with FA and found that 1) the fundamental genetic defect in FA impairs skeletal muscle OXPHOS and 2) the number of GAA triplet repeats is inversely proportional to skeletal muscle OXPHOS[33]. More recently, Nachbauer *et al.* used PMRS as a secondary outcome measure in an FA drug trial with 7 subjects. PCr recovery times were significantly longer in subjects compared to controls, reaffirming Lodi's earlier work and indicating that the effects of aberrant frataxin expression in FA can result in a decline in mitochondrial capacity that is detectable using PMRS techniques[58].

Reliable methods to adequately define *in vivo* skeletal muscle function in a feasible, cost-effective, and reproducible manner are critical to improving subject outcomes in a range of diseases that affect mitochondrial function.

This work outlines a robust procedure for obtaining *in vivo* maximum oxidative capacity of skeletal muscle using ^{31}PMRS. The in-magnet exercise protocol is well tolerated by individuals spanning a wide range of physical and functional abilities and affords a simplified subject setup using inexpensive and widely-available equipment.

Protocol

This protocol is approved by and follows the guidelines of the Ohio State University Institutional Review Board for human subjects research. It is critically important that all procedures involving MR equipment are performed by adequately trained personnel adhering to the highest standards of MR safety[59].

1. Materials and Preparation

1. Ensure that all necessary materials are available prior to the experiment (**Figure 2**).
2. Plug the ^{31}P coil into the in-table coil connector at the end of the exam table closest to the bore. Place a large triangle foam cushion near the head of the MR exam table, but not directly on the ^{31}P coil. Place a head pillow at the other end of the MR exam table, farthest from the bore, for subject comfort.

2. Subject Positioning (Figure 3a)

1. Instruct the subject to lie supine, feet first on the MR table. Place a foam cushion under the knees to support the leg in a partially flexed position.
2. Position the subject close to the right side of the table (the subject's right) in order to center the left thigh as closely to the magnet isocenter as possible, thus ensuring optimal B0 homogeneity in the thigh muscle under examination. Provide the subject with ear plugs and/or headphones.
3. Position the ^{31}P RF coil on the left quadriceps at approximately the midpoint between the patella and the femoral head, and secure to the leg using straps. Place the coil over the lateral portion of the leg, above the vastus lateralis.
4. Secure the baby oil to the medial aspect of the thigh with the same straps used to secure the coil to the leg. This facilitates scan localization.
5. Bind the subject's legs together with a strap placed below the coil and above the knee. Secure the subject's legs to the MR table with additional straps, one above the knee and one midway between the knee and ankle.
6. Use the laser light guide to delineate the center of the coil and move the table to the magnet isocenter using this centering landmark.

3. Exercise Protocol

1. Explain to the subject that the exercise protocol consists of three phases: an initial, baseline phase; a short, intense exercise phase; and a recovery phase.
2. Instruct the subject to lie still and relax their leg muscles during the baseline and recovery phases of the spectroscopy acquisition in order to minimize motion artifacts.
3. Provide a countdown to the subject indicating the start of exercise. At this point, have the subject initiate knee extension/flexion as forcefully and as rapidly as possible against the resistance of the straps.
   NOTE: The quadriceps muscles are used to move the left lower leg up and down, until instructed to stop.
4. Terminate exercise after a 30% drop in the PCr peak height.
   1. Observe the PCr peak height in the acquisition viewer window, and also view it upon completion of the exercise sequence.
      NOTE: A general guideline is that an approximate 30% drop in PCr peak height corresponds to a Pi peak that is 50% of the height of the PCr peak. If PCr depletion is not occurring rapidly enough to achieve a 30% drop during the exercise phase of the exam, encourage the subject to kick harder or faster while exercising.
      NOTE: Cessation of exercise is determined by monitoring the PCr peak height and duration of exercise. This may result in slightly different durations of exercise in different patients and can be accounted for in the analysis.

4. Scan Protocol

1. Acquire a tri-plane localizer to verify proper subject positioning and identify the location of the ^{31}P coil.
   NOTE: The localizer sequence begins automatically and centers at the indicated position using the laser light guide (step 2.9)
2. Acquire a second tri-plane localizer.
   1. Open the slice view on the first tri-plane localizer images.
      NOTE: This process may be different for different software and hardware systems.
   2. Center and rotate the slice orientation by left-clicking and holding on the slice group. Rotate the slice group. Ensure that the final orientation of slices matches with the position of the baby oil.
   3. In the sequence routine window, increase the number of slices to cover the entire leg in the axial and sagittal images (**Figure 3b**).
3. [31]P spectroscopy sequence:

1. Use the following non-localized pulse-acquire sequence parameters: TR: 1,000 msec; TE: 0.34 msec; spectral width: 2,000 Hz; flip angle: 90 degrees; acquired data points: 1,024; 4 averages resulting in a time resolution of 1 spectrum every 6 sec.

4. ^{31}P shim box placement:
   1. Using a mouse, drag the second triplane localizer images into the viewing window at the top of the screen. Drag the spectroscopy sequence into the protocol window and double-click to open.
   2. Use the position tool bar to visualize the shim voxel (select the black rectangle with horizontal lines). After selecting this option, observe a green box on the localizer images.
      NOTE: This is the shim voxel.
   3. Move the voxel by left-clicking and holding the voxel in the center. Change the size and rotate the orientation of the voxel by left-clicking and holding the voxel at the corner of the box. Place the shim box so as to ensure B0 field homogeneity directly below the coil and parallel to the plane of the quadriceps.
      NOTE: This is to ensure proper shimming within the sensitive region under the coil, which is the volume of tissue directly below the center of the coil.
   4. Use the tri-plane localizer images to identify the sensitive region of the coil and adjust the shim box to encompass this region within the quadriceps muscle.
      NOTE: The shim box can be larger than the true coverage of the surface coil in order to ensure B0 homogeneity within the data acquisition voxel (**Figure 3c**).
5. ^{31}P test acquisition:
   1. Open the acquisition viewer window and select the head icon in the acquisition tool bar. This will allow for viewing of the spectroscopy acquisition in real time.
   2. After placement of the 31P shim voxel, run the sequence to obtain a single spectrum by clicking the "run" button at the top of the protocol window.
   3. Examine the quality of B0 shimming. Observe the resulting spectrum in the acquisition window. Observe a prominent PCr peak centered at 0 ppm and no significant noise (**Figure 4a**, left).
      NOTE: Troubleshooting: If the spectrum appears noisy, ensure that the shim box is placed within muscle. Adjust the size and position of the shim box to improve the signal-to-noise ratio. Repeat the test acquisition as needed.
   4. In order to see the PCr peak height, open the spectrum in the spectroscopy tool ("Applications" → "Spectroscopy"). Open the patient's folder (folder tree icon), select the appropriate scan, and double-click to load the spectrum.

5. Pre-exercise T1 image:
   1. Obtain a single-slice axial T1-weighted image at the center of a coil.

6. ^{31}P pre-exercise acquisition:
   1. Copy the sequence from step 4.4 (that produced the best spectral quality) by left-clicking and dragging the sequence in the protocol window. Use this sequence for all subsequent measurements.
   2. In the sequence routine window, increase the number of measurements from 1 to 10. Select run to acquire 10 measurements while the subject is at rest.

7. ^{31}P exercise acquisition:
   NOTE: Make careful note of the start and end exercise times, as this will be important for analysis.
   1. Rest: Apply the shim settings from the previous scan and set the sequence to acquire 20 measurements. Instruct the subject to begin kicking after a countdown. Instruct the subject to remain at rest for 2 measurements.
   2. Exercise: Ask the subject to perform the knee extension exercise for ~ 30 sec (or the time required to achieve a 30% decrease in the PCr peak amplitude). After the subject achieves sufficient PCr depletion, ask them to rest.

8. ^{31}P post-exercise acquisitions:
   1. Acquire an additional 20 measurements at rest. Ensure that the post-exercise acquisitions begin immediately following the exercise sequence, without pause or shimming (**Figure 4a**, right).
      NOTE: The subdivision of this recovery period into two separate acquisitions permits the analysis of the initial 20 dynamic spectra during the acquisition of the second 20 dynamic spectra, allowing the operator to avoid acquisition of the full recovery period if the exercise needs to be repeated.

9. Ensuring exercise quality:
   1. Compare the PCr peak heights at the beginning and end of exercise. High-quality exercise sessions result in a ~ 30% decrease in the PCr concentration.
   2. Verify that the PCr peak height is the same at beginning of rest and at the end of recovery (typically, < 10% difference is desired). This ensures that there was negligible loss of field homogeneity during acquisition.
      NOTE: If the PCr breakdown is insufficient, or if there has been a loss of field homogeneity, then repeat the exercise/recovery portion of the exam (taking care to avoid fatigue), ensure that the coil and straps are securely attached, and extend the duration of exercise and/or encourage more vigorous exercise (**Figure 4b**).
      NOTE: A comparison of the images obtained in steps 6 and 11 permits an additional quality control step to visualize any displacement of the thigh and coil due to the exercise, thus ensuring that minimal motion occurred during the protocol, which could significantly affect the acquired data.

10. Following post-exercise T1 imaging, repeat the pre-exercise axial T1 imaging (step 4.5) using the same acquisition parameters.
    1. In addition to sufficient depletion of PCr, measure the end exercise pH to ensure that the exercise did not induce acidosis of the muscle.
    2. Perform this by measuring the chemical shift between Pi and PCr (δP_i) and using the following equation[60]:
       $$pH = 6.77 + \log[(\delta P_i\text{-}3.29)/(5.68\text{-}\delta P_i)]$$

NOTE: The pH should remain greater than 6.8[61]. If the PCr breakdown is sufficient but the pH is too low, repeat the exercise bout for a shorter duration and/or with a decreased intensity.

11. Saving Data:
 1. Save all acquired spectra as DICOM files and export them for processing using JMRUI.
 2. If using a scanner, select all spectroscopy acquisitions in the "Navigator" window.
 3. Under "Applications," select "Dicom Tools" → "Export MR Spectroscopy," and save the DICOM (*.dcm) files to C:/User/MedCom/temp/ CDROFFLINE
    (the tool automatically chooses this location).
 4. Under "Transfer," select "Export to Offline." Save to the desired location.

5. Data Processing and Analysis[62]

1. Analyze the MR spectra with freely-available JMRUI software (version 5.2; http://www.jmrui.eu/).
2. Apodize and phase shift the spectra to ensure uniformity over all acquired time points (**Figure 5**). The PCr peak will be centered at 0 ppm in the spectra.
3. Use the built-in AMARES algorithm to quantify the amplitude of the PCr peak in each acquired spectrum. The peak amplitude represents the concentration of PCr within the sensitive region of the surface coil at that particular time point.
4. In the computational software, plot the PCr concentrations as a function of acquisition time. Using the built-in computational software curve-fit tool, fit the PCr recovery period data to the following equation[52,63]:

$$PCr(t) = PCr_0 + PCr_\Delta * e^{\frac{1}{\tau}}$$

5. Record the values of the baseline PCr ($PCr_0 + PCr_\Delta$), the lowest PCr (PCr_Δ), and the recovery time (τ).
6. Ensure that the appropriate conditions are met during the exercise session by calculating the PCr depletion, the percent difference between the baseline PCr and the lowest PCr. Ideal exercise sessions result in a 20 - 50% depletion.
NOTE: The quality of the curve fitting can be ensured by verifying that the R^2 value is greater than 0.75. R^2 values are automatically calculated by the fitting software.

Representative Results

Reproducibility Study

Six volunteers (4 men and 2 women; mean age: 24.5 ± 6.2 years) with no self-reported heart, metabolic, or mitochondrial disease underwent sessions of the described ^{31}PMRS exercise and imaging technique on 2 different days within 1 week to evaluate technique reproducibility (**Figure 6a**). The studies performed on normal volunteers confirm the reproducibility of the ^{31}PMRS study in the quantification of mitochondrial function. A Bland-Altman analysis of PCr recovery time demonstrates a mean difference standard deviation of 1.03 4.83 sec and a between-trials coefficient of variation of 4.66 (**Figure 6b**). No changes to the acquisition or analysis protocol described in the methods section were required to obtain good-quality data, as described in step 4 of the protocol. These results demonstrate the reproducibility of the acquisition and analysis techniques described in this work.

Technique Evaluation in Non-ambulatory Participants with Friedrich's Ataxia

Four participants (2 men and 2 women; mean age: 35) underwent a single session of the ^{31}PMRS exercise and imaging technique described in this work to evaluate its feasibility in a non-ambulatory population with FA. These subjects were capable of performing the in-magnet exercises for obtaining sufficient depletion of PCr to fit the recovery parameters shown in step 5.6. However, longer exercise times (60 - 90 sec) were required to sufficiently deplete the PCr levels. Additionally, oscillations around the fit that were caused by the progressive loss of muscle control, which is characteristic of this disease, were noted (**Figure 7**). For these subjects, we used two additional resistive straps between the knees and ankles, giving a total of three straps, to limit unwanted motion. These results demonstrate the feasibility of the acquisition and analysis technique to obtain PCr recovery times in non-ambulatory subjects. However, the modifications required to obtain good-quality data indicate that further evaluation and standardization studies are necessary.

Feasibility Study

Nine volunteers with no self-reported cardiovascular disease and 15 subjects referred to a program of cardiac rehabilitation and secondary prevention (CRSP) were enrolled in a local institutional review board (IRB)-approved study. We obtained some clinical values as indicators of cardiovascular health and severity of metabolic syndrome. The left ventricular ejection fraction was preserved in CRSP subjects (56 10%). The maximum cardiovascular exertion ability, measured before starting CRSP, was similar in subjects with and without diabetes (3.05 0.6 *versus* 3.4 0.8 metabolic equivalents METs, p = 0.4). Prior to starting CRSP, each enrolled subject underwent the ^{31}PMRS exercise and imaging technique, described in this work, and the intramuscular fat quantification imaging, described previously[64]. The time constant of PCr recovery was longer (41.9 1.4 *versus* 32.1 7.4 sec, p = 0.05), and the intramuscular fat percentage was higher in CRSP subjects versus controls (8.7 2.9 *versus* 2.54 0.6%, p < 0.001). The percentage of intramuscular fat was similar in CRSP subjects with and without diabetes (p = 0.4), and the time constant of PCr recovery tended to be longer in subjects with diabetes versus in those without diabetes and in controls (p = 0.03 for the trends across groups). Preliminary follow-up data suggest a considerably worse improvement in METs post-CRSP in subjects with diabetes compared to those without (delta = 1.0 0.8 versus 4.0 2.4, p = 0.06; **Figure 8**). These results demonstrate the feasibility of this technique to quantify differences in skeletal muscle OXPHOS between subjects with and without known metabolic disease.
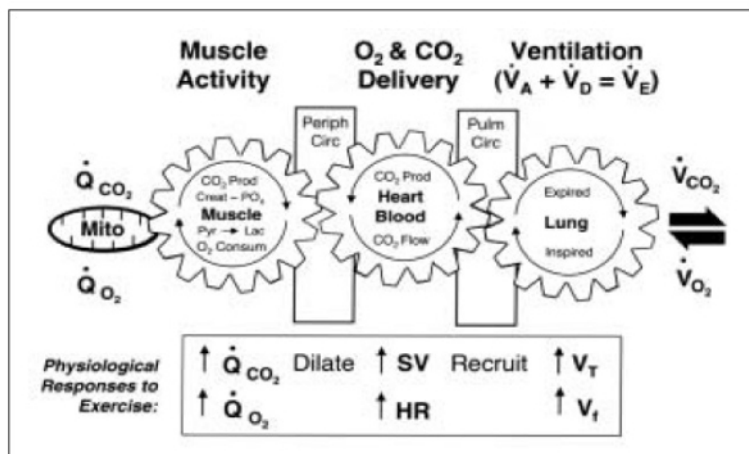
Figure 1. Mitochondria, Skeletal Muscle, and Cardiopulmonary Systems.
A representation of the link between mitochondria, skeletal muscle, cardiac output, ventilation, and functional capacity is shown. Reproduced from Milani *et al*[65].
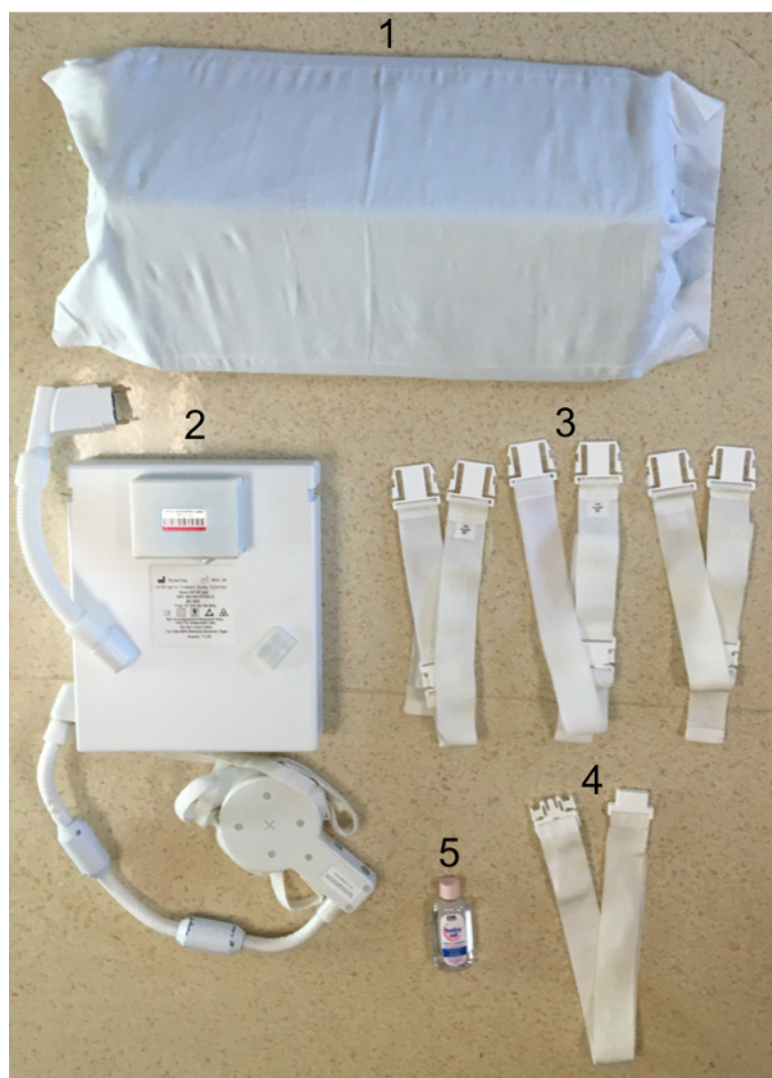

Figure 2. Materials.
The required materials include **1)** a triangle cushion, **2)** a 10-cm ^{31}P-tuned transmit-receive surface coil, **3)** table-to-table connecting resistive straps, **4)** a self-connecting resistive strap, and **5)** a small bottle of baby oil. Please click here to view a larger version of this figure.
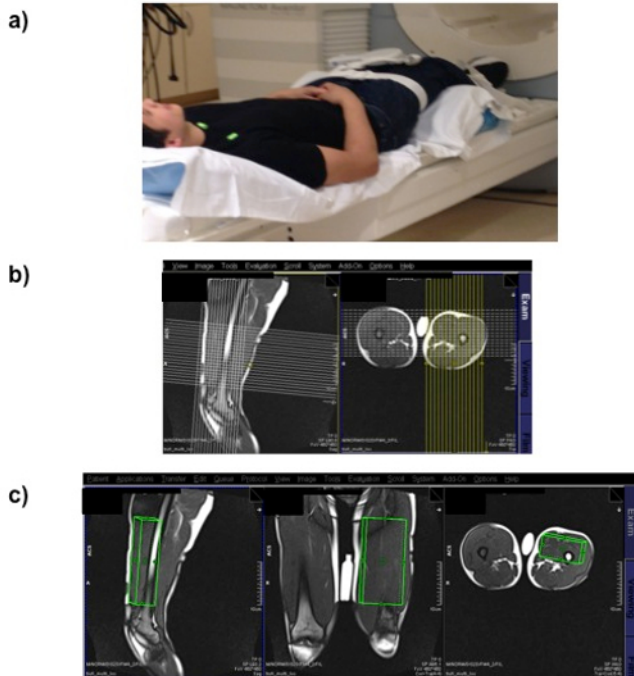
Figure 3. Positioning.
A) Subjects are imaged in a supine, feet-first position. The ^{31}P coil is placed on the left quadriceps. Resistive straps are placed above and below the knee and attached to the table. A single strap is used to bind both legs together above the knee. **B)** The slice positioning is shown for the second localizer. Note that the slices are centered at the location of the baby oil bottle, and slices cover the entire quadriceps. **C)** The shim box placement for ^{31}PMRS is shown. This volume is placed directly below the coil in the quadriceps and covers a depth that insures sufficient signal and appropriate shimming within the area of the surface coil.
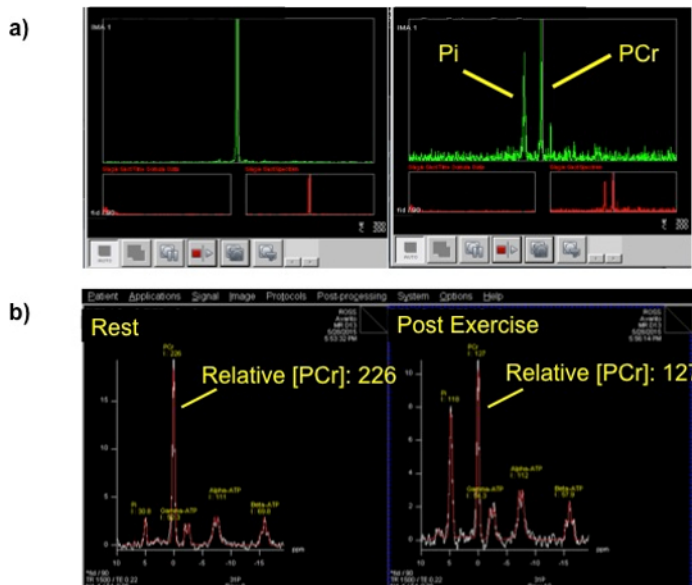

Figure 4. Data Acquisition.
A) A representative ^{31}P acquisition at rest is shown. The PCr is the large single peak, and there is minimal noise (left). A typical acquisition during the exercise portion of the protocol results in two large peaks, Pi and PCr (right). As exercise progresses, the Pi and PCr peaks will increase and decrease, respectively. **B)** Comparison of the PCr peak height at rest and post-exercise should reveal at least a ~30% decrease. This calculation should be done at the scanner console in order to ensure the successful completion of the exercise study.
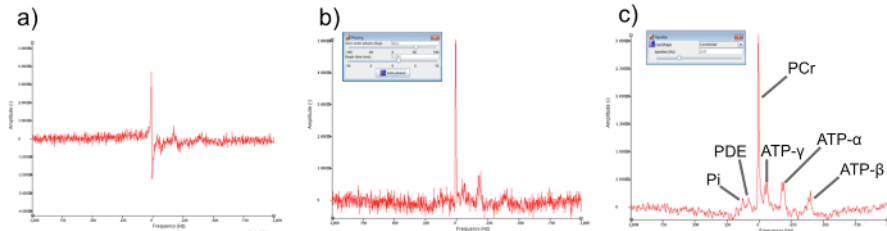
Figure 5. Analysis.
The phase correction and apodization of a representative spectrum is shown. **A)** A raw spectrum showing an un-phased peak and the presence of noise that obscures the peaks. **B)** A spectrum showing 0th- and 1st-order phase correction. The PCr peak located at the center frequency is easily identifiable, but other metabolite peaks are still obscured. **C)** The spectrum after apodization with a Lorentzian line shape, resulting in a reduction in noise and better visualization of the 3 ATP peaks and the PDE and Pi peak. This spectrum is ready for peak quantification with the AMARES tool. Please click here to view a larger version of this figure.
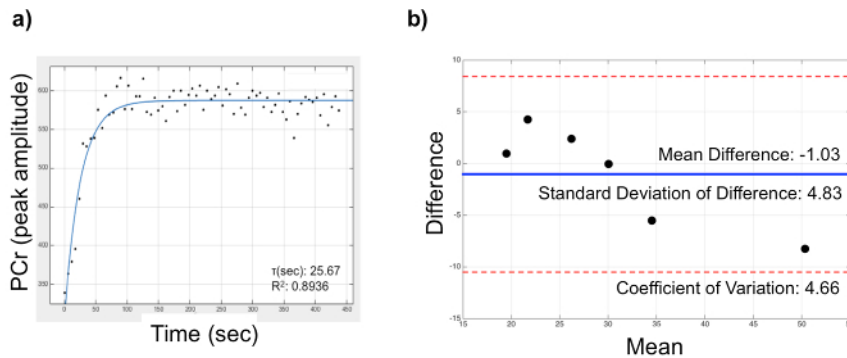

Figure 6. ^{31}PMRS in Healthy Subjects.
A) This figure shows the recovery of the phosphocreatine (PCr) concentration after its depletion with rapid quasi-static knee extension exercise. The line represents the fit of the exponential recovery function described in step 5.6, with the recovery time constant τ shown; this time constant is a well-established biomarker of mitochondrial oxidative function. **B)** The Bland-Altman analysis of the ^{31}PMRS technique reproducibility demonstrates a mean difference standard deviation of 1.03 4.83 sec for the PCr recovery time between trials; the coefficient of variation is 4.66. Please click here to view a larger version of this figure.
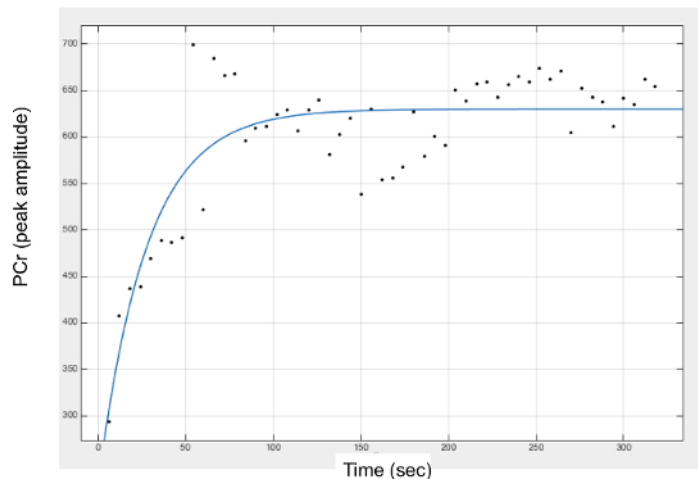

Figure 7. ^{31}PMRS in Non-ambulatory Subjects.
A representative PCr recovery curve from the ^{31}PMRS examination of a non-ambulatory subject is shown. Note that a PCr depletion of 64% was attained with this exercise protocol. Please click here to view a larger version of this figure.
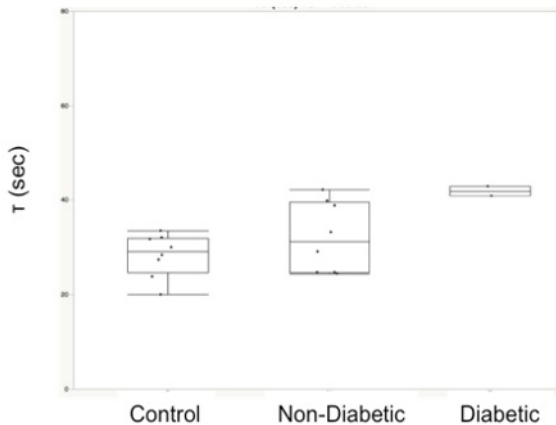
Figure 8. ^{31}PMRS in CRSP Subjects.
A comparison of PCr recovery times demonstrates sequentially poorer mitochondrial oxidative capacity in control, non-diabetic, and diabetic subjects. The error bars represent the standard deviation.

Discussion

This paper describes a standard protocol for ^{31}PMRS examination that affords serial and noninvasive *in vivo* measurement of skeletal muscle mitochondrial function. The protocol holds considerable appeal when considering the breadth of investigations targeting the growing burden of metabolic syndrome and its resulting morbidity and mortality. This ^{31}PMRS protocol requires a minimal amount of scanner time and can be incorporated into comprehensive metabolic investigations in subjects at any center with commercially-available MRS facilities.

Critical Steps within the Protocol

Contraindications- Prior to MR examinations, it is crucial to screen subjects for potential contraindications. In addition to typical MR exclusion criteria, the following should be considered before implementing this protocol: 1) ipsilateral knee or hip implants (regardless of MR compatibility) to avoid artifacts, 2) conditions that restrict blood flow or oxygen delivery to the lower limbs (*e.g.,* peripheral artery disease), 3) an inability to perform resistive quadriceps extension exercise, and 4) an inability to lie supine for approximately 30 min.

Motion artifact reduction- The movement of the ^{31}P coil with respect to the subject's quadriceps and the movement of the subject's thigh relative to the table should be minimized. Ensure that the coil is securely fastened to the subject's leg and that that the resistive straps are securely fastened to the exam table. Test this by ensuring that the subject's heel rises no more than 5 in. off the exam table during kicking and that there is no rotation of the coil during the exercise.

Acquisition

Exercise Quality- The subject should exercise to achieve at least a 30% depletion in the PCr. For this protocol, we have determined that 30 s of exercise for ambulatory subjects and 60 s for non-ambulatory subjects achieves this target. We have observed that non-ambulatory subjects exert less force per kick and therefore require a longer interval for sufficient depletion.

Analysis- The methods described here provide a framework to minimize the subjectivity and maximize the automation. Selection of user input parameters for the analysis of the spectra should be made carefully in order to ensure reproducibility.

Modifications and Troubleshooting

Quality of Spectrum- If the spectrum appears noisy, ensure that the shim box is placed within muscle. Adjust the size and position of the shim box to improve the signal-to-noise ratio. Repeat the test acquisition as needed.

Quality of Exercise- If the initial exercise results in insufficient PCr depletion, there are several modifications that can be used to troubleshoot: 1) the straps can be tightened, to increase resistance; 2) the subject can be instructed to kick faster, which increases exertion; or 3) the duration of sustained exercise can be increased. However, note that over-exercise can result in altered pH and could lead to acidosis, which can inhibit the OXPHOS recovery kinetics[61]. This can be avoided by limiting the exercise time to a maximum of 3 min.

Limitations of the Technique

A muscle biopsy analysis permits the measurement of specific mitochondrial characteristics, such as mitochondrial content and size, as well as the mitochondrial maximum ATP synthesis rate. However, it is important to note that the *in vivo* measurement using ^{31}PMRS represents an aggregate of these direct measures, in addition to extra-mitochondrial factors, such as the microvascular supply of oxygenated blood to the muscle. Thus, in situations where the status of the microvasculature is in question due to reduced oxygen supply or other factors, it would not provide an unambiguous indicator of mitochondrial function. Rather, it would indicate the *in vivo* status of the maximum oxidative ATP synthesis of muscle, which may reflect some combination of OXPHOS and microvascular issues.

A limitation of the exercise ^{31}PMRS protocol detailed in this work is the lack of standardization of work output. This lack of standardization simplifies the apparatus required, and thus the implementation of this protocol. However, it comes at the expense of not permitting the

quantitative evaluation of other parameters, such as strength and fatigability, and their relationship to metabolic measures. As a result, varying levels of exertion could impact the PCr recovery time beyond the severity of the underlying mitochondrial defect. One can minimize these effects by ensuring sufficient PCr depletion and can further standardize the work output by using MR-compatible ergometers with adjustable resistance and measurable work outputs.

Significance of the Technique with Respect to Existing or Alternative Methods

The ability to directly quantify mitochondrial function in skeletal muscle is the main advantage of the ^{31}PMRS technique when compared to standard metabolic exercise testing. Invasive muscle biopsy affords measurements in single fibers[66], though with attendant risks that make it less appealing for investigations requiring serial assessment. Approaches based on near-infrared spectroscopy[67] may be limited by penetration depth, particularly in obese patients, where as little as 5 mm of fat attenuates the NIRS signal by 20%[68]. Furthermore, the technique does not lend itself to the multidimensional assessment of muscle and other systems afforded by MR-based techniques. Additionally, unlike invasive biopsy methods for quantifying muscle energetics, this non-invasive and non-destructive measure permits repeated measures of the metabolic status in intact muscle, making it advantageous for the evaluation of subject populations and therapeutic interventions.

Future Applications

Potential applications after mastering this ^{31}PMRS technique include the evaluation of diseases with specific mitochondrial defects or any of a broad range of metabolic disorders. In patients with poor cardiac output, current techniques can identify impaired functional capacity but cannot establish the level at which the dysfunction occurs (*e.g.,* the skeletal muscle, heart, or lungs). It would be particularly interesting to develop integrated protocols that combine ^{31}PMRS with metabolic measures and cardiopulmonary assays to identify the root causes of subject-specific reduced capacity in order to facilitate personalized therapies.

We have detailed examples of important targeted therapies and interventions that would benefit from the use of *in vivo* markers of mitochondrial function. A standardized ^{31}PMRS exercise protocol, such as the one detailed above, is an important step for more widespread use of this important *in vivo* marker of skeletal muscle mitochondrial capacity in both basic and intervention studies.

Disclosures

The authors have nothing to disclose.

Acknowledgements

References

1. Eckel, R. H., Alberti, K. G., Grundy, S. M., & Zimmet, P. Z. The metabolic syndrome. *Lancet.* **375** (9710), 181-183 (2010).
2. Shulman, G. I. Ectopic fat in insulin resistance, dyslipidemia, and cardiometabolic disease. *N Engl J Med.* **371** (12), 1131-1141 (2014).
3. Holmstrom, M. H., Iglesias-Gutierrez, E., Zierath, J. R., & Garcia-Roves, P. M. Tissue-specific control of mitochondrial respiration in obesity-related insulin resistance and diabetes. *Am J Physiol Endocrinol Metab.* **302** (6), E731-739 (2012).
4. Jheng, H. F. *et al.* Mitochondrial fission contributes to mitochondrial dysfunction and insulin resistance in skeletal muscle. *Mol Cell Biol.* **32** (2), 309-319 (2012).
5. Petersen, K. F. *et al.* Mitochondrial dysfunction in the elderly: possible role in insulin resistance. *Science.* **300** (5622), 1140-1142 (2003).
6. Kelley, D. E., He, J., Menshikova, E. V., & Ritov, V. B. Dysfunction of mitochondria in human skeletal muscle in type 2 diabetes. *Diabetes.* **51** (10), 2944-2950 (2002).
7. Liu, R. *et al.* Impaired mitochondrial dynamics and bioenergetics in diabetic skeletal muscle. *PLoS One.* **9** (3), e92810 (2014).
8. Ha, H., Hwang, I. A., Park, J. H., & Lee, H. B. Role of reactive oxygen species in the pathogenesis of diabetic nephropathy. *Diabetes Res Clin Pract.* **82 Suppl 1** S42-45 (2008).
9. Akude, E. *et al.* Diminished superoxide generation is associated with respiratory chain dysfunction and changes in the mitochondrial proteome of sensory neurons from diabetic rats. *Diabetes.* **60** (1), 288-297 (2011).
10. Fernyhough, P. Mitochondrial dysfunction in diabetic neuropathy: a series of unfortunate metabolic events. *Curr Diab Rep.* **15** (11), 89 (2015).
11. Chen, M., Wang, W., Ma, J., Ye, P., & Wang, K. High glucose induces mitochondrial dysfunction and apoptosis in human retinal pigment epithelium cells via promoting SOCS1 and Fas/FasL signaling. *Cytokine.* **78** 94-102 (2016).
12. Blake, R., & Trounce, I. A. Mitochondrial dysfunction and complications associated with diabetes. *Biochim Biophys Acta.* **1840** (4), 1404-1412 (2014).
13. Rains, J. L., & Jain, S. K. Oxidative stress, insulin signaling, and diabetes. *Free Radic Biol Med.* **50** (5), 567-575 (2011).
14. Serviddio, G. *et al.* Mitochondrial involvement in non-alcoholic steatohepatitis. *Mol Aspects Med.* **29** (1-2), 22-35 (2008).
15. Perez-Carreras, M. *et al.* Defective hepatic mitochondrial respiratory chain in patients with nonalcoholic steatohepatitis. *Hepatology.* **38** (4), 999-1007 (2003).
16. Garcia-Ruiz, I. *et al.* Mitochondrial complex I subunits are decreased in murine nonalcoholic fatty liver disease: implication of peroxynitrite. *J Proteome Res.* **9** (5), 2450-2459 (2010).
17. Patti, M. E., & Corvera, S. The role of mitochondria in the pathogenesis of type 2 diabetes. *Endocr Rev.* **31** (3), 364-395 (2010).
18. Muoio, D. M., & Newgard, C. B. Obesity-related derangements in metabolic regulation. *Annu Rev Biochem.* **75** 367-401 (2006).
19. Bonnard, C. *et al.* Mitochondrial dysfunction results from oxidative stress in the skeletal muscle of diet-induced insulin-resistant mice. *J Clin Invest.* **118** (2), 789-800 (2008).

20. Jheng, H. F., Huang, S. H., Kuo, H. M., Hughes, M. W., & Tsai, Y. S. Molecular insight and pharmacological approaches targeting mitochondrial dynamics in skeletal muscle during obesity. *Ann N Y Acad Sci.* **1350** 82-94 (2015).

21. Coen, P. M., & Goodpaster, B. H. Role of intramyocelluar lipids in human health. *Trends Endocrinol Metab.* **23** (8), 391-398 (2012).

22. Montgomery, M. K., & Turner, N. Mitochondrial dysfunction and insulin resistance: an update. *Endocr Connect.* **4** (1), R1-R15 (2015).

23. Martelli, A., & Puccio, H. Dysregulation of cellular iron metabolism in Friedreich ataxia: from primary iron-sulfur cluster deficit to mitochondrial iron accumulation. *Front Pharmacol.* **5** 130 (2014).

24. Campuzano, V. *et al.* Frataxin is reduced in Friedreich ataxia patients and is associated with mitochondrial membranes. *Hum Mol Genet.* **6** (11), 1771-1780 (1997).

25. Calabrese, V. *et al.* Oxidative stress, mitochondrial dysfunction and cellular stress response in Friedreich's ataxia. *J Neurol Sci.* **233** (1-2), 145-162 (2005).

26. Ristow, M. *et al.* Frataxin activates mitochondrial energy conversion and oxidative phosphorylation. *Proc Natl Acad Sci U S A.* **97** (22), 12239-12243 (2000).

27. Ardehali, H. *et al.* Targeting myocardial substrate metabolism in heart failure: potential for new therapies. *Eur J Heart Fail.* **14** (2), 120-129 (2012).

28. Ren, J., Pulakat, L., Whaley-Connell, A., & Sowers, J. R. Mitochondrial biogenesis in the metabolic syndrome and cardiovascular disease. *J Mol Med (Berl).* **88** (10), 993-1001 (2010).

29. Marin-Garcia, J., & Goldenthal, M. J. Understanding the impact of mitochondrial defects in cardiovascular disease: a review. *J Card Fail.* **8** (5), 347-361 (2002).

30. Babcock, M. *et al.* Regulation of mitochondrial iron accumulation by Yfh1p, a putative homolog of frataxin. *Science.* **276** (5319), 1709-1712 (1997).

31. Foury, F., & Cazzalini, O. Deletion of the yeast homologue of the human gene associated with Friedreich's ataxia elicits iron accumulation in mitochondria. *FEBS Lett.* **411** (2-3), 373-377 (1997).

32. Wardman, P., & Candeias, L. P. Fenton chemistry: an introduction. *Radiat Res.* **145** (5), 523-531 (1996).

33. Lodi, R. *et al.* Cardiac energetics are abnormal in Friedreich ataxia patients in the absence of cardiac dysfunction and hypertrophy: an in vivo 31P magnetic resonance spectroscopy study. *Cardiovasc Res.* **52** (1), 111-119 (2001).

34. Raman, S. V. *et al.* Impaired myocardial perfusion reserve and fibrosis in Friedreich ataxia: a mitochondrial cardiomyopathy with metabolic syndrome. *Eur Heart J.* **32** (5), 561-567 (2011).

35. Kitzman, D. W. *et al.* Skeletal muscle abnormalities and exercise intolerance in older patients with heart failure and preserved ejection fraction. *Am J Physiol Heart Circ Physiol.* **306** (9), H1364-1370 (2014).

36. Scheuermann-Freestone, M. *et al.* Abnormal cardiac and skeletal muscle energy metabolism in patients with type 2 diabetes. *Circulation.* **107** (24), 3040-3046 (2003).

37. Allcock, D. M., & Sowers, J. R. Best strategies for hypertension management in type 2 diabetes and obesity. *Curr Diab Rep.* **10** (2), 139-144 (2010).

38. Katzmarzyk, P. T., Church, T. S., Janssen, I., Ross, R., & Blair, S. N. Metabolic syndrome, obesity, and mortality: impact of cardiorespiratory fitness. *Diabetes Care.* **28** (2), 391-397 (2005).

39. Wang, J. *et al.* The metabolic syndrome predicts cardiovascular mortality: a 13-year follow-up study in elderly non-diabetic Finns. *Eur Heart J.* **28** (7), 857-864 (2007).

40. Zambon, S. *et al.* Metabolic syndrome and all-cause and cardiovascular mortality in an Italian elderly population: the Progetto Veneto Anziani (Pro.V.A.) Study. *Diabetes Care.* **32** (1), 153-159 (2009).

41. Malik, S. *et al.* Impact of the metabolic syndrome on mortality from coronary heart disease, cardiovascular disease, and all causes in United States adults. *Circulation.* **110** (10), 1245-1250 (2004).

42. Ropper, A. H., & Samuels, M. A. *Adams and Victor's Principles of Neurology.* 9 edn, The McGraw-Hill Companies,Inc, (2009).

43. Abeti, R. *et al.* Targeting lipid peroxidation and mitochondrial imbalance in Friedreich's ataxia. *Pharmacol Res.* **99** 344-350 (2015).

44. Li, Y. *et al.* Excision of Expanded GAA Repeats Alleviates the Molecular Phenotype of Friedreich's Ataxia. *Mol Ther.* **23** (6), 1055-1065 (2015).

45. Toledo, F. G., & Goodpaster, B. H. The role of weight loss and exercise in correcting skeletal muscle mitochondrial abnormalities in obesity, diabetes and aging. *Mol Cell Endocrinol.* **379** (1-2), 30-34 (2013).

46. Oldridge, N. B., Guyatt, G. H., Fischer, M. E., & Rimm, A. A. Cardiac rehabilitation after myocardial infarction. Combined experience of randomized clinical trials. *JAMA.* **260** (7), 945-950 (1988).

47. O'Connor, G. T. *et al.* An overview of randomized trials of rehabilitation with exercise after myocardial infarction. *Circulation.* **80** (2), 234-244 (1989).

48. Ryan, T. E., Brizendine, J. T., & McCully, K. K. A comparison of exercise type and intensity on the noninvasive assessment of skeletal muscle mitochondrial function using near-infrared spectroscopy. *J Appl Physiol (1985).* **114** (2), 230-237 (2013).

49. Wallimann, T. Bioenergetics. Dissecting the role of creatine kinase. *Curr Biol.* **4** (1), 42-46 (1994).

50. Forbes, S. C., Paganini, A. T., Slade, J. M., Towse, T. F., & Meyer, R. A. Phosphocreatine recovery kinetics following low- and high-intensity exercise in human triceps surae and rat posterior hindlimb muscles. *Am J Physiol Regul Integr Comp Physiol.* **296** (1), R161-170 (2009).

51. Korzeniewski, B., & Rossiter, H. B. Each-step activation of oxidative phosphorylation is necessary to explain muscle metabolic kinetic responses to exercise and recovery in humans. *J Physiol.* **593** (24), 5255-5268 (2015).

52. Meyer, R. A. A linear model of muscle respiration explains monoexponential phosphocreatine changes. *Am J Physiol.* **254** (4 Pt 1), C548-553 (1988).

53. McCully, K. K., Fielding, R. A., Evans, W. J., Leigh, J. S., Jr., & Posner, J. D. Relationships between in vivo and in vitro measurements of metabolism in young and old human calf muscles. *J Appl Physiol (1985).* **75** (2), 813-819 (1993).

54. Layec, G., Haseler, L. J., & Richardson, R. S. Reduced muscle oxidative capacity is independent of O2 availability in elderly people. *Age (Dordr).* **35** (4), 1183-1192 (2013).

55. Larson-Meyer, D. E., Newcomer, B. R., Hunter, G. R., Hetherington, H. P., & Weinsier, R. L. 31P MRS measurement of mitochondrial function in skeletal muscle: reliability, force-level sensitivity and relation to whole body maximal oxygen uptake. *NMR Biomed.* **13** (1), 14-27 (2000).

56. Kemp, G. J., Ahmad, R. E., Nicolay, K., & Prompers, J. J. Quantification of skeletal muscle mitochondrial function by 31P magnetic resonance spectroscopy techniques: a quantitative review. *Acta Physiol (Oxf).* **213** (1), 107-144 (2015).

57. Lynch, D. R. *et al.* Near infrared muscle spectroscopy in patients with Friedreich's ataxia. *Muscle Nerve.* **25** (5), 664-673 (2002).

58. Nachbauer, W. *et al.* Bioenergetics of the calf muscle in Friedreich ataxia patients measured by 31P-MRS before and after treatment with recombinant human erythropoietin. *PLoS One.* **8** (7), e69229 (2013).

59. Kanal, E. *et al.* ACR guidance document on MR safe practices: 2013. *J Magn Reson Imaging.* **37** (3), 501-530 (2013).

60. Petroff, O. A., Ogino, T., & Alger, J. R. High-resolution proton magnetic resonance spectroscopy of rabbit brain: regional metabolite levels and postmortem changes. *J Neurochem.* **51** (1), 163-171 (1988).

61. Jubrias, S. A., Crowther, G. J., Shankland, E. G., Gronka, R. K., & Conley, K. E. Acidosis inhibits oxidative phosphorylation in contracting human skeletal muscle in vivo. *J Physiol.* **553** (Pt 2), 589-599 (2003).

62. Layec, G. *et al.* Reproducibility assessment of metabolic variables characterizing muscle energetics in vivo: A 31P-MRS study. *Magn Reson Med.* **62** (4), 840-854 (2009).

63. Iotti, S., Lodi, R., Frassineti, C., Zaniol, P., & Barbiroli, B. In vivo assessment of mitochondrial functionality in human gastrocnemius muscle by 31P MRS. The role of pH in the evaluation of phosphocreatine and inorganic phosphate recoveries from exercise. *NMR Biomed.* **6** (4), 248-253 (1993).

64. Wren, T. A., Bluml, S., Tseng-Ong, L., & Gilsanz, V. Three-point technique of fat quantification of muscle tissue as a marker of disease progression in Duchenne muscular dystrophy: preliminary study. *AJR Am J Roentgenol.* **190** (1), W8-12 (2008).

65. Milani, R. V., Lavie, C. J., Mehra, M. R., & Ventura, H. O. Understanding the basics of cardiopulmonary exercise testing. *Mayo Clin Proc.* **81** (12), 1603-1611 (2006).

66. Wust, R. C., van der Laarse, W. J., & Rossiter, H. B. On-off asymmetries in oxygen consumption kinetics of single Xenopus laevis skeletal muscle fibres suggest higher-order control. *J Physiol.* **591** (3), 731-744 (2013).

67. Ryan, T. E., Brophy, P., Lin, C. T., Hickner, R. C., & Neufer, P. D. Assessment of in vivo skeletal muscle mitochondrial respiratory capacity in humans by near-infrared spectroscopy: a comparison with in situ measurements. *J Physiol.* **592** (15), 3231-3241 (2014).

68. Hamaoka, T., McCully, K. K., Niwayama, M., & Chance, B. The use of muscle near-infrared spectroscopy in sport, health and medical sciences: recent developments. *Philos Trans A Math Phys Eng Sci. '3.* **69**, 4591-4604 (2011).